Effect of strain path change on texture evolution of AZ91 magnesium alloy under rolling.

Biplab Mohapatra, Ajay Majhee

College of Engineering Bhubaneswar, Biju Pattnaik University of Technology, Odisha, India

Abstract

In the current work, hot cross rolling (CR) and unidirectional rolling (UR) of a typical AZ91 alloy were used to systematically study the texture evolution and mechanical anisotropy. The outcomes demonstrate how much the rolling path influences the annealed texture. A texture with basal poles primarily distributed along the transverse direction (TD) develops in the UR. On the other hand, following hot cross rolling and annealing, an ellipse-like (0002) texture with a basal pole that slopes mostly away from the normal direction (ND) develops. As a result, the CR is a useful technique for customizing the experimental alloy's texture. Sadly, this ellipse-like texture was unable to hold its shape during the unidirectional hot rolling and annealing that followed. Comparing UR and CR plates to conventional unidirectional rolled plates reveals a significant planar mechanical anisotropy.

1. Introduction

Because of the need for weight reduction in manufacturing, magnesium alloys are being used more and more in the aerospace and transportation industries [1]. However, because of their strong basal texture formation and limited slip systems, magnesium alloys show strong anisotropy and poor ductility at low and/or room temperature [2–5]. A number of techniques, including texture modification, temperature elevation, and grain refinement, have been used to increase the formability of magnesium plates [6, 7].

One method for changing the texture is to add rare-earth (RE) elements or calcium to magnesium alloy [8–10]. This has been shown to be a successful way to improve the ductility and formability at room temperature [11,12]. Weak textures with basal poles tilting away from the normal direction (ND) to the transverse direction (TD) are typically developed in magnesium alloys with a certain number of diluted concentrations of RE or Ca elements along with zinc. These alloys showed high elongations and excellent formability at room temperature [8,11–15]. The double-peak textured plates exhibit a notable planar mechanical anisotropy, which may lead to notable variations in ductility and strength when applied external stress along the rolling direction (RD) or the TD, respectively. As a result, during the forming process, it is simple to generate earrings, which is a drawback for practical application [16].

Certain specialized processing techniques, including torsion extrusion and equal channel angular extrusion (ECAE) [17–19], have been shown to be successful in creating weak (0002) basal textures in magnesium alloys. However, these processing technologies require more frequent intrusion because they are not continuous. Furthermore, the sample size is extremely small. By comparison, the rolling process is easy to control and less efficient due to these drawbacks. Additionally, it has been stated that annealing after cross rolling alternately along

the RD and TD is a valid method for improving the formability of aluminum AA5182 plates by customizing the texture [20]. Consequently, it most likely demonstrates how closely the strain path and texture evolution are related. In a prior study, Wang et al. discovered that altering the rolling directions of Mg–5Li–1Al–0.5Y alloy as it is rolled can refine the grain size and has a noticeable impact on its mechanical properties and texture [21]. Therefore, given that magnesium alloys containing calcium may weaken the basal texture following hot deformation, it is intriguing to investigate whether hot cross rolling could produce the same result in inexpensive magnesium-zinc-ca alloy plates [22, 23].

The microstructure and texture evolution of AZ91 alloy plates during various hot rolling processes were examined in the current study. In addition, the purpose of the mechanical property tests was to investigate the correlation between texture type and mechanical property in various orientations. The related mechanisms were examined and talked about.

2. Experimental Procedure

The first plate, which has a thickness of 3 mm and a relative coarse grain and random texture, was created using some AZ91plates that were homogenized and as-cast (Fig. 1a and b). The first plate was hot rolled at 400 °C and reduced by 20% overall using two distinct rolling techniques: cross rolling (CR) and unidirectional rolling (UR). Cross rolling (CR), as shown in Fig. 2, is the rolling path being alternately altered by 90° on each pass along the RD and TD. Unidirectional rolling (UR), on the other hand, refers to multi-pass unidirectional hot rolling that always occurs along the RD. In this instance, the homogenized plate's first pass rolling direction was RD, and its transverse direction was TD. The rolled plates

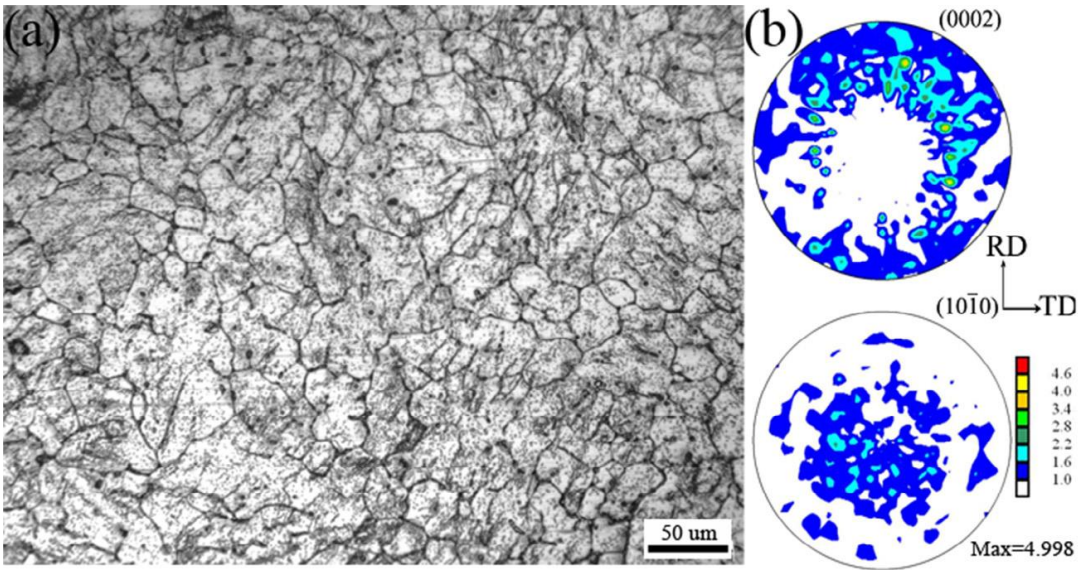

Fig. 1. (a) Optical micrographs in the RD–ND plane and (b) XRD pole figures of the homogenized AZ91 plate.

were then annealed for two hours at 400 °C in order to obtain a completely recrystallized microstructure. After that, the two annealed plates—referred to as UR–RD and CR–RD,

respectively—were multi-pass hot rolled along the RD at a constant 15% total reduction. Here, we kept the rolling and annealing temperatures constant with what was previously stated.

Utilizing optical microscopy (ZEISS, Axiovert 40 MAT), the microstructure was investigated. Using EBSD (FEI NOVA400 SEM with Oxford-EBSD system) and X-ray diffraction (XRD, Rigaku D/max-2500PC), the texture was measured in the center of the RD-TD plane. After determining the orientation distribution function from the measured incomplete pole figures, the complete pole figures were rebuilt.

The annealed plates were machined into dog-bone tension specimens measuring 14 mm in gauge length, 4 mm in gauge width, and 1.8 mm in gauge thickness. At room temperature, tension tests were conducted along the RD, 45°, and TD using a strain rate of 1×10^{-3} s^{-1} on a Shimadzu mechanical testing system [24] (Fig. 3). Using the average value of the three tests, the ultimate tensile strength, yield strength, and elongation were determined.

3. Results and discussions

3.1. Microstructure

The optical microstructures of the hot-rolled AZ91 plates in the RD–ND plane are shown in Fig. 4. The CR sample shows small shear bands, which are made up of numerous twins and dislocations, as shown in Fig. 4a. Fig. 4c illustrates the microstructures of the UR sample, where dense typical shear bands are visible. Moreover, because there are more grain nucleation sites in dense shear bands, the grain size in the UR sample is significantly smaller than the grain size in the CR sample. Similar microstructures with some dense shear bands and clearly elongated deformed grains along the rolling direction are depicted in Figs. 4b and d. Furthermore, Fig. 4b–d shows a deformed microstructure with some grains that are partially elongated along the RD. It is evident that all of the plates have a large number of tiny dynamic recrystallization grains as a result of the hot rolling.

The annealed plates' EBSD microstructure produces a fully recrystallized structure in every plate, as shown in Fig. 5. Figures 5a–d show average grain sizes of approximately 38 μm, 37 μm, 38 μm, and 35 μm, respectively.

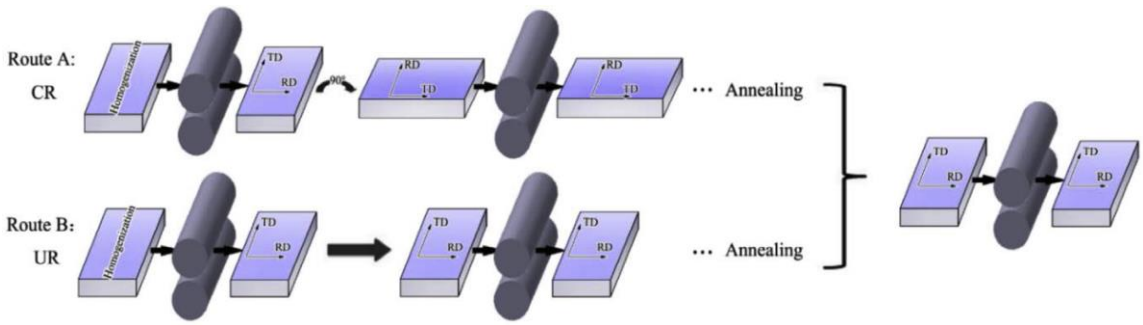

Fig. 2. Schematic diagrams showing the two different hot rolling processes.

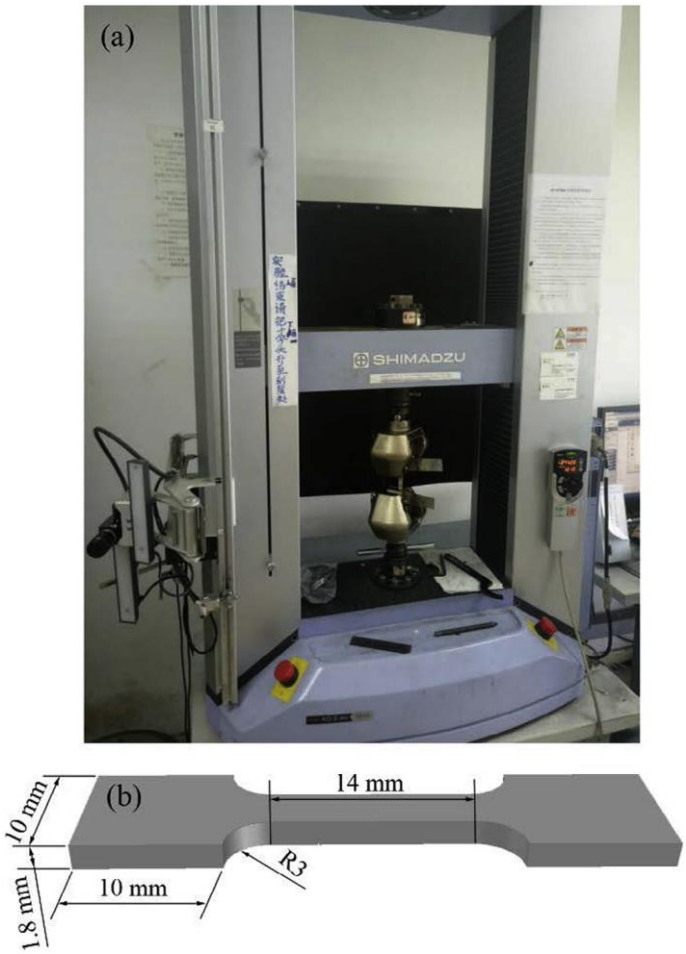

Fig. 3. Equipment and sample geometry for mechanical tests.

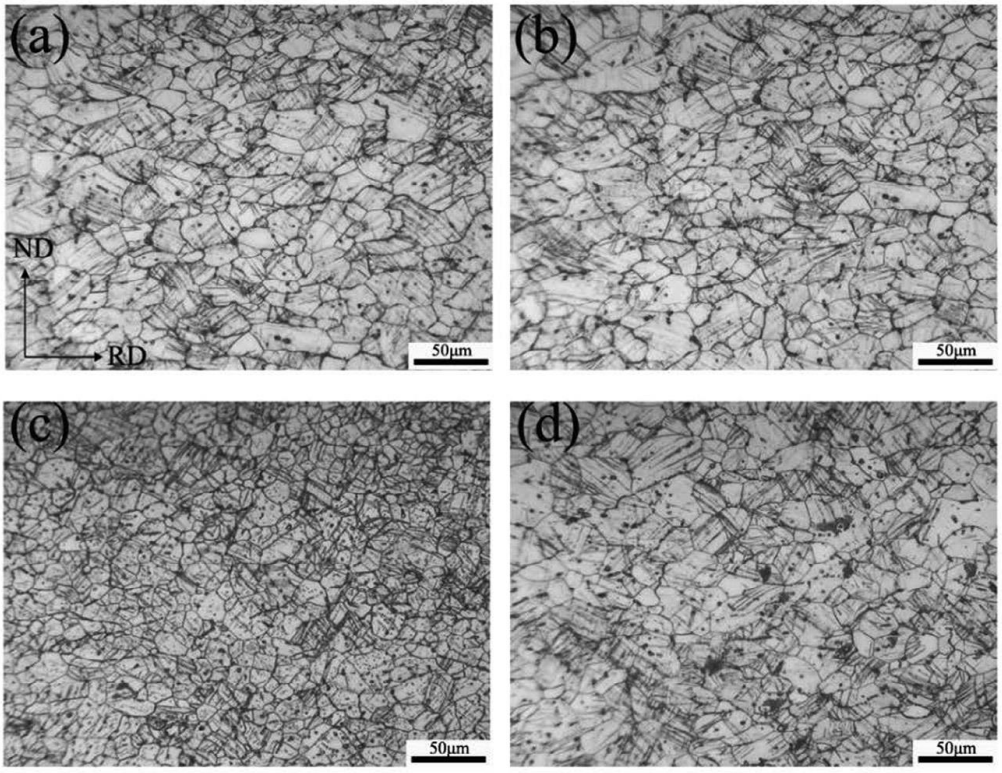

Fig. 4. Optical micrographs of AZ91 plates after different hot rolling processes at 400 °C: (a) CR; (b) CR–RD; (c) UR; (d) UR–RD.

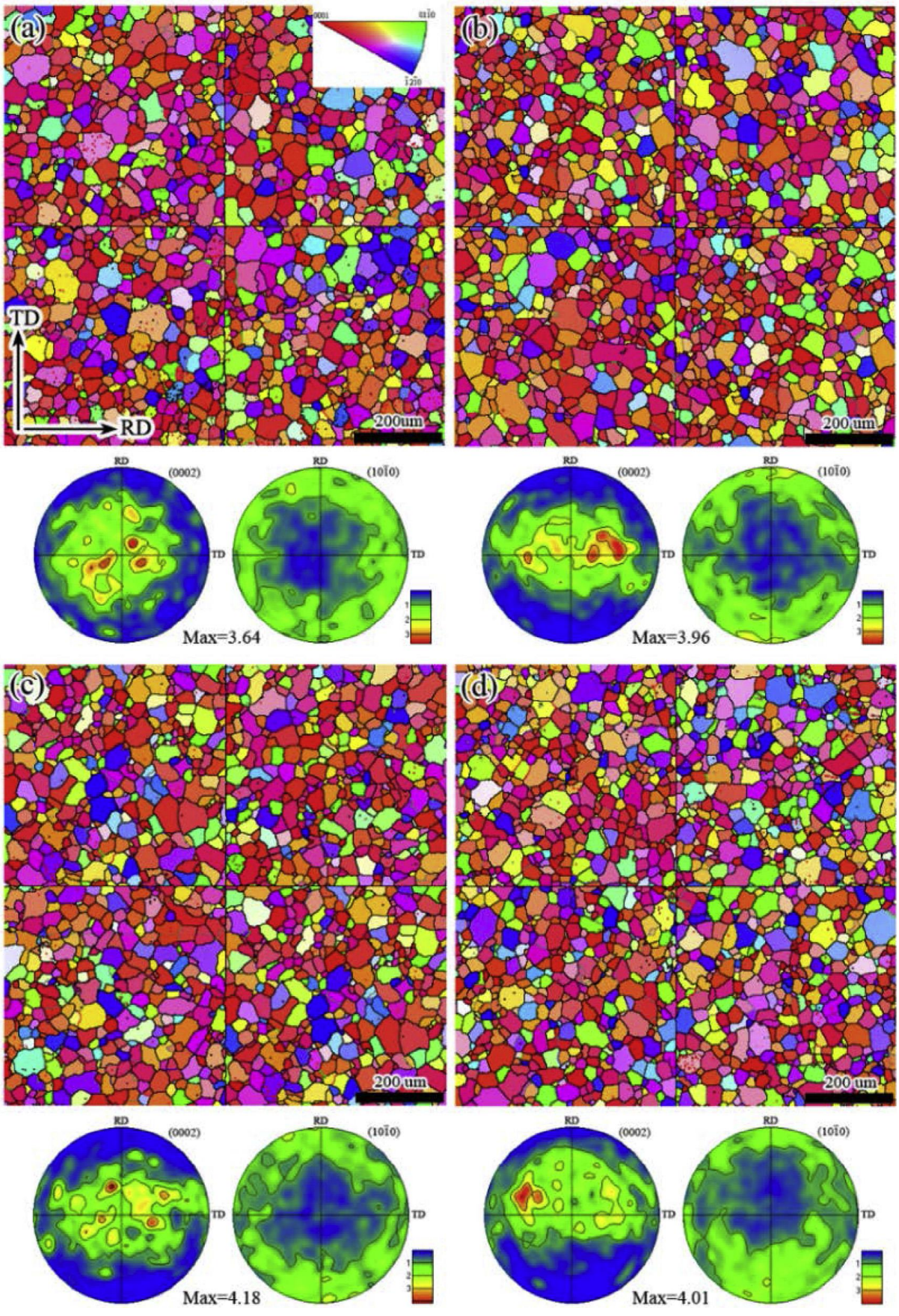

Fig. 5. Inverse pole figure maps and pole figure maps obtained from the hot rolled samples after annealing at 400 °C for 2 h: (a) CR; (b) CR–RD; (c) UR; (d) UR–RD.

3.2. Texture Evolution

Fig. 6 displays the XRD pole figures of the hot-rolled AZ91 plates both before and after they were annealed for two hours at 400 °C. Following hot rolling, it displays textures with basal poles tilting from ND to TD. A weaker texture with a basal pole in the CR plate, as shown in Fig. 6a, displays an ellipsoidal form of the intensity distribution and is reserved following annealing. The peak intensities that are tilting toward TD and RD are slightly higher than each other. There is a slight increase in maximum intensity from 2.306 to 2.715.

As opposed to this, Fig. 6c depicts a typical double peak TD-split texture in the UR plate that is located around 20° away from the ND and retains its texture type after further annealing. The results mentioned above are nearly identical to those found in the earlier study [22]. On the other hand, the maximum texture intensity rises to 3.270 from 2.706. The TD-split double-peak texture is developed in both the CR-RD and UR-RD plates before and after annealing, as seen in Figs. 6b and d. It resembles the UR plate in that regard. The EBSD pole figure maps that were obtained from the hot rolled samples following a 2-hour annealing at 400 °C are in line with the previously reported findings, as can be observed in Fig. 5.

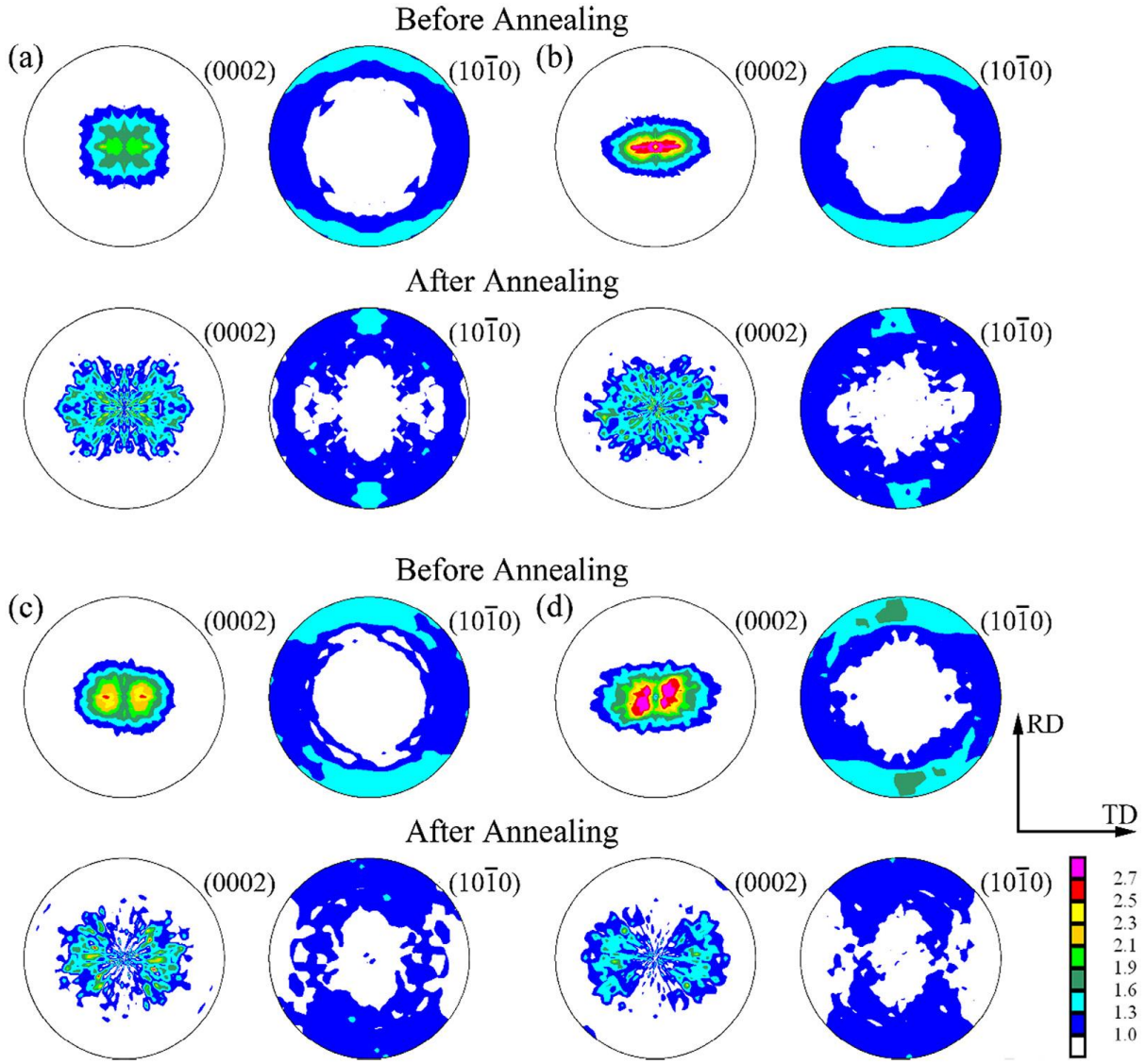

Fig. 6. Pole figures of the hot rolled AZ91 plates before and after annealing at 400 °C for 2 h: (a) CR; (b) CR–RD; (c) UR and (d) UR–RD.

Naturally, the texture can be efficiently tailored both before and after annealing by changing the hot rolling path.CR is a useful technique for creating a random texture with basal poles dispersing as an oval and almost homogeneous crystallographic orientations, as demonstrated in Figs. 5a and 6a. This outcome nearly agrees with the findings of the earlier research [25]. It follows that in magnesium alloys with basal poles that largely tilt away from the ND, such as RE-containing or Ca-containing Mg–Zn alloys, CR may modify the texture components considerably [26–28].

An analysis of the CR and UR rolled plates is presented here because it's interesting to see how the textures evolved during the rolling processes due to various deformation mechanisms. Both CR and UR cause the basal poles to incline toward the ND, as shown in Figs. 6a and c. Since the initial plate's grain basal poles are mostly located away from the ND, there is a lot of basal slip activity during both CR and UR. It is believed that basal slip is primarily responsible for this rotation of basal poles toward the ND. On the other hand, the typical TD-split double-peak texture seen in the UR rolled plate gives way to an ellipsoidal (0002) texture in the CR rolled AZ91 plate.

Furthermore, Fig. 4 illustrates that there are significantly more twins in the UR plate than in the CR plate, indicating a greater significance of twinning in the UR process. The distribution of (0002) texture along the RD differs from that along the TD because the rolling path of UR is constant (along the RD). Slip system activation becomes challenging, and as deformation increases, twining becomes the dominant mechanism, producing numerous twins and noticeable shear bands. Since CR has rolling paths along both the RD and TD, the stress concentration in the localized region is reduced and the slip systems along both directions should initiate, resulting in uniform deformation and fewer twins. As a result, the distribution of basal poles in the CR rolled plate takes the form of an ellipse as peaks of the basal poles incline toward both the RD and the TD. The distribution of the basal poles created in the preceding rolling pass may change when the rolling path is changed, which could be the cause. In fact, non-basal slips exhibit high activity when AZ91 plate is hot-rolled [29]. As can be seen in Fig. 6, some deformed grains exhibit a slightly different distribution, but their basal poles clearly incline about 20° away from the ND spreading along the RD. Pyramidal <c+a > slip was activated during the rolling of AZ31 plates, which resulted in the basal poles spreading from the ND toward the RD [30]. We therefore suspect that the texture in our current

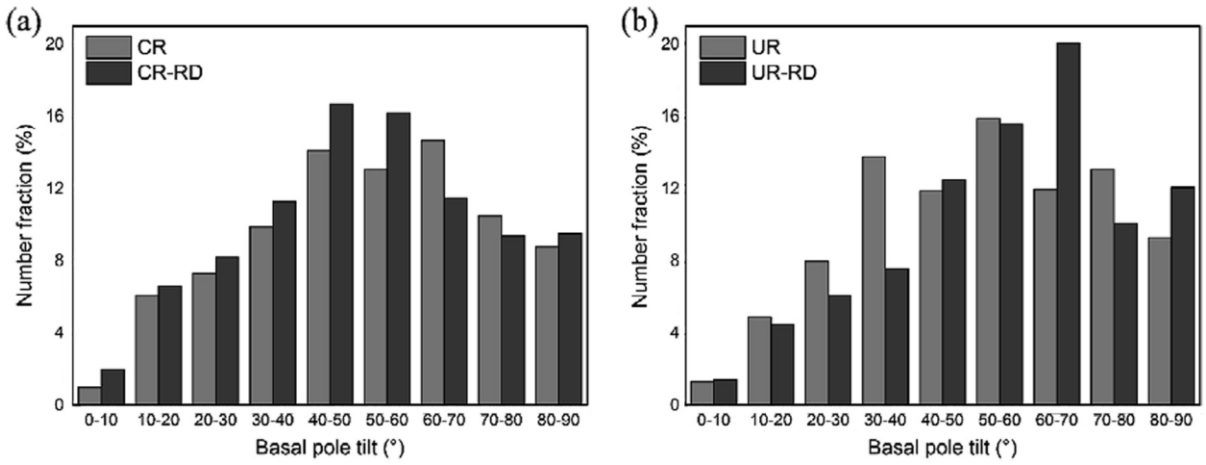

Fig. 7. Quantitative statistics histograms of the relative different orientations of basal poles obtained from the hot rolled sample after full recrystallization annealing: (a) CR and CR–RD; (b) UR and UR–RD.

study fits this explanation.

Further subarea statistical analysis was carried out in this study for recrystallized grains based on the size and orientation of basal poles away from ND toward RD/TD. It can unequivocally confirm if the ellipsoidal texture created by CR after annealing can be saved for the UR that follows annealing. In order to achieve a more dependable outcome, each inverse pole figure (IPF) was calculated using more than 1500 grains by measuring the EBSD data of annealing plates containing fully recrystallized grains (Fig. 5).

The quantitative statistical histograms of the relative orientations of the basal poles in each annealed plate are displayed in Fig. 7, and they show the texture evolution's tendency. Most of the grains in the annealed CR plate have basal poles that tilt between 40 and 70 degrees away from ND. These grains can be classified as having an off-basal orientation, which refers to the development of a non-basal texture, as suggested by Basu and Al-Samman [27] and illustrated in Fig. 5a. On the other hand, the annealed CR-RD plate exhibits a higher frequency of tilting within the 40–60° range, leading to an elevated maximum intensity.

Furthermore, compared to CR (Figs. 5a and c), the distribution of basal poles toward TD in the subsequent uniaxial rolled plates following annealing is more noticeable. The annealed CR-RD and CR plate show quantified measurements of 67.8% of TD-split grains compared to 52.3% for each. Meanwhile, the texture of UR plates appears to be unchanged, with basal poles primarily inclining about 30–60° away from ND for the cogging specimen and 60–70° for the UR-RD, as shown in Fig. 7b. It goes without saying that annealing could weaken each plate's strong basal texture, albeit at various angles and directions of inclination. The quantity variance of grain orientation between RD and TD could only be eliminated by CR followed by annealing, producing a uniform distribution. Sadly, after further rolling and annealing, this ellipsoidal texture could not be inherited.

3.3. Mechanical Properties

Tension tests were used to measure the mechanical properties of the annealed plate along the RD, TD, and 45° away from the RD. The results are shown in Fig. 8. For the annealed CR–RD plate, Fig. 8b demonstrates the significant variation in elongation and yield strength along the various directions. The yield strength along the RD is approximately 23 MPa higher than that along the TD. Additionally, between those along the RD and TD, the yield strength along the 45°away from the RD acts as a mediator. The elongation in various directions, however, reveals a contrary trend. The characteristic double-peak texture of annealed UR-RD plates exhibits this phenomenon as well. Evidently, these findings show that the macroscopic mechanical behaviors during tensile tests were significantly impacted by the basal pole splitting toward the TD. The texture in this instance shows that the basal poles spread more toward the TD than the RD (Figs. 5b and d). As a result, the plates typically have a significant degree of planar mechanical anisotropy. In actuality, the (0002) texture and the activity of various slip systems in magnesium alloy plates are closely correlated. Along the planar TD, slip systems—especially basal slip—are far more active than they are along the RD. As a result, the yield strength would be reduced and fewer stresses would be required in the transverse direction. Furthermore, it is noteworthy that the sample orientation has no discernible impact on the ultimate tensile strength (US), which is in line with the findings in references [11,16,26,31].

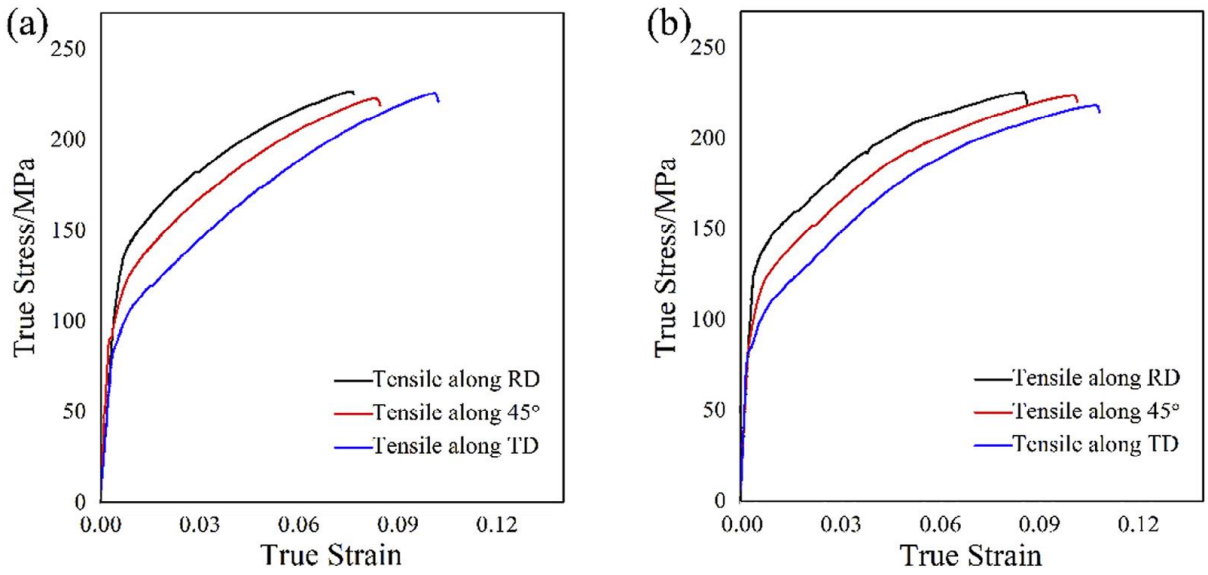

Fig. 8. True stress–strain curves along different directions of (a) UR–RD and (b) CR–RD hot rolled AZ91 plates after annealing at 400 °C for 2h.

4. Conclusion

The evolution of the AZ91 binary alloy's microstructure and texture was examined in the current study. The following is a summary of the primary conclusions:

1. The hot-rolled AZ91 plate's optical microstructures reveal that the UR sample has significantly more shear bands than the CR sample does over the whole RD–ND. Additionally, the UR sample's grain size distribution was more homogeneous than the CR sample's, which is mostly explained by the increased grain nucleation in dense shear bands.
2. It was discovered that the annealing texture, whose basal poles uniformly distribute on an ellipse away from the ND, is significantly impacted by the hot cross rolling stage. However, after further unidirectional hot rolling and annealing, the cross-rolled annealing texture was unable to reserve.
3. The results of mechanical property tests indicate that there is a significant variation in the yield strength and elongation of the annealed plates along the RD, TD, and 45° away from the RD. In the CR-RD annealed plate, yield strength (elongation) along the RD is roughly 23 MPa (2.3%) higher (lower) than that along the TD, which is fairly similar to that obtained in the UR-RD annealed plate.

References

1. H. Yan, S.W. Xu, R.S. Chen, S. Kamado, T. Honma, E.H. Han, J. Alloys Compd. 566 (2013) 98–107.
2. Y. Chino, K. Kimura, M. Mabuchi, Mater. Sci. Eng. A 486 (2008) 481–488.
3. S.R. Agnew, Ö. Duygulu, Int. J. Plast 21 (2005) 1161–1193.

4. Y. Xin, M. Wang, Z. Zeng, G. Huang, Q. Liu, Scr. Mater. 64 (2011) 986–989.
5. M. Kavyani, G.R. Ebrahimi, M. Sanjari, M. Haghshenas, J. Magn. Alloys 4 (2016) 89–98.
6. W.J. Kim, S.I. Hong, Y.S. Kim, S.H. Min, H.T. Jeong, J.D. Lee, Acta Mater. 51 (2003) 3293–3307.
7. H. Koh, T. Sakai, H. Utsunomiya, S. Minamiguchi, Mater. Trans. 48 (2007) 5.
8. J. Bohlen, M.R. Nürnberg, J.W. Senn, D. Letzig, S.R. Agnew, Acta Mater. 55 (2007) 2101–2112.
9. Y. Chino, M. Kado, M. Mabuchi, Mater. Sci. Eng. A 494 (2008) 343–349.
10. Z.R. Zeng, M.Z. Bian, S.W. Xu, C.H.J. Davies, N. Birbilis, J.F. Nie, Scr. Mater. 108 (2015) 6–10.
11. H. Yan, R.S. Chen, E.H. Han, Mater. Charact. 62 (2011) 321–326.
12. Y. Chino, K. Sassa, M. Mabuchi, Mater. Sci. Eng. A 513–514 (2009) 394–400.
13. J. Wendt, K.U. Kainer, G. Arruebarrena, K. Hantzsche, J. Bohlen, D. Letzig, Magnesium Technology 2009, TMS, San Francisco, 2009, pp. 289–293.
14. L. Mackenzie, M. Pekguleryuz, Scr. Mater. 59 (2008) 665–668.
15. J. Wang, X. Zhang, X. Lu, Y. Yang, Z. Wang, J. Magnes. Alloys 4 (2016) 207–213.
16. D. Wu, R.S. Chen, E.H. Han, J. Alloys Compd. 509 (2011) 2856–2863.
17. S.R. Agnew, J.A. Horton, T.M. Lillo, D.W. Brown, Scr. Mater. 50 (2004) 377–381.
18. X. Huang, K. Suzuki, A.Watazu, I. Shigematsu, N. Saito, Mater. Sci. Eng. A 48 (2008) 8214–8220.
19. Y. Chino, K. Sassa, M. Mabuchi, Scr. Mater. 59 (2008) 399–402.
20. M.Y. Huh, S.Y. Cho, O. Engler, Mater. Sci. Eng. A 315 (2001) 17.
21. T. Wang, T. Zhu, J. Sun, R. Wu, M. Zhang, J. Magnes. Alloys 3 (2015) 345–351.
22. K. Illkova, P. Dobronˇ, F. Chmelík, K.U. Kainer, J. Balík, S. Yi, et al., J. Alloys Compd. 617 (2014) 253–264.
23. N. Stanford, Mater. Sci. Eng. A 528 (2010) 314–322.
24. ASTM E21-09, Standard Test Methods for Elevated Temperature Tension Tests of Metallic Materials, Annual Book of ASTM Standards, vol. 03.01, 2009.
25. J. Bohlen, J. Wendt, M. Nienaber, K.U. Kainer, L. Stutz, D. Letzig, Mater. Charact. 101 (2015) 144–152.
26. H. Yan, R.S. Chen, E.H. Han, Mater. Sci. Eng. A 527 (2010) 3317–3322.
27. I. Basu, T. Al-Samman, Acta Mater. 67 (2014) 116–133.
28. Y. Chino, X. Huang, K. Suzuki, K. Sassa, M. Mabuchi, Mater. Sci. Eng. A 528 (2010) 566–572.
29. S. Kleiner, P.J. Uggowitzer, Mater. Sci. Eng. A 379 (2004) 258–263.
30. A. Styczynski, C. Hartig, J. Bohlen, D. Letzig, Scr. Mater. 50 (2004) 943–947.
31. S. Pan, Y. Xin, G. Huang, Q. Li, F. Guo, Q. Liu, Mater. Sci. Eng. A 653 (2016) 93–98.